Appendices for "Coherent Lagrangian vortices: The black holes of turbulence"

G. Haller[1] and F. J. Beron-Vera[2]

[1]Institute for Mechanical Systems, ETH Zurich, Zurich, Switzerland

[2] Rosenstiel School of Marine and Atmospheric Science, University of Miami, Miami FL, USA

Appendix A. Euler-Lagrange equations for the average strain Q

The Euler-Lagrange equations for stationary values for the averaged Lagrangian strain Q are of the form

$$\partial_r \sqrt{\frac{\langle r', C_{t_0}^t(r)r'\rangle}{\langle r', r'\rangle}} - \frac{\mathrm{d}}{\mathrm{d}s}\partial_{r'}\sqrt{\frac{\langle r', C_{t_0}^t(r)r'\rangle}{\langle r', r'\rangle}} = 0. \tag{A 1}$$

We introduce the index notation C_{ij} for the coordinate representation of the tensor $C_{t_0}^t$, and r_j for the components of the vector r. Then the equation can be written out in the coordinate form

$$\frac{C_{ij,m}(r)r_i'r_j'}{2\sqrt{C_{ij}(r)r_i'r_j'r_k'r_k'}} - \frac{\mathrm{d}}{\mathrm{d}s}\frac{C_{mj}(r)r_j'r_k'r_k' - C_{ij}(r)r_i'r_j'r_m'}{\sqrt{C_{ij}(r)r_i'r_j'(r_k'r_k')^3}} = 0, \tag{A 2}$$

using the summation convention over repeated indices. Carrying out the differentiation $\frac{\mathrm{d}}{\mathrm{d}s}$ in (A 2) leads to the final, lengthy form of the Euler–Lagrange equations, which will be omitted here for brevity.

Appendix B. Stationary curves of the averaged strain are Green–Lagrange null-geodesics

By classic results in the calculus of variations (Gelfand & Fomin 2000), stationary points of the averaged strain functional Q are trajectories of (A 1). With the shorthand notation

$$A(r, r') = \langle r', C_{t_0}^t(r)r'\rangle, \quad B(r') = \langle r', r'\rangle, \tag{B 1}$$

Q can be rewritten as

$$Q(\gamma) = \frac{1}{\sigma}\int_0^\sigma \sqrt{\frac{A(r, r')}{B(r')}}\, \mathrm{d}s, \tag{B 2}$$

while its Euler–Lagrange equations (A 1) as

$$\partial_r\sqrt{\frac{A}{B}} - \frac{\mathrm{d}}{\mathrm{d}s}\partial_{r'}\sqrt{\frac{A}{B}} = 0. \tag{B 3}$$

Note that

$$\partial_r\sqrt{\frac{A}{B}} = \frac{\partial_r A}{\sqrt{AB}}, \quad \partial_{r'}\sqrt{\frac{A}{B}} = \frac{1}{B}\left[\frac{\partial_{r'}A}{\sqrt{A}}\sqrt{B} - \frac{\partial_{r'}B}{\sqrt{B}}\sqrt{A}\right]. \tag{B 4}$$

Since the integrand of $Q(\gamma)$ has no explicit dependence on the parameter s, Noether's

theorem (Gelfand & Fomin 2000) guarantees the existence of a first integral for (B 3). This integral can be computed as

$$I = \sqrt{\frac{A}{B}} - \left\langle r', \partial_{r'} \sqrt{\frac{A}{B}} \right\rangle = \sqrt{\frac{A}{B}} = I_0 = \text{const}, \tag{B 5}$$

where we have used the specific form of the functions A and B from (B 1), as well as the second equation from (B 4).

With the notation $\lambda = I_0 > 0$, we therefore have the identity

$$A(r(s), r'(s)) \equiv \lambda^2 B\left(r'(s)\right) \tag{B 6}$$

on any solution (B 3) for some appropriate value of the positive constant $\lambda > 0$. Therefore, all solutions of (B 3) are uniformly λ-stretching.

To obtain further insight into these solutions, we use the identity (B 6) to rewrite the expressions (B 4) as

$$\partial_r \sqrt{\frac{A}{B}} = \frac{1}{2\lambda B} \partial_r A, \quad \partial_{r'} \sqrt{\frac{A}{B}} = \frac{1}{2\lambda B} \partial_{r'} \left[A - \lambda^2 B\right]. \tag{B 7}$$

We also introduce a rescaling of the independent variable s in equation (B 3) via the formula

$$\frac{\mathrm{d}\tau}{\mathrm{d}s} = B(r'(s)), \tag{B 8}$$

which, by the chain rule, implies

$$B(r'(s)) = \frac{1}{B(\dot{r}(\tau))}, \tag{B 9}$$

with the dot referring to differentiation with respect to the new variable τ. Note that $B(r'(s))$ is nonvanishing on smooth curves with well-defined tangent vectors, and hence the change of variables (B 8) is well defined.

After the $s \mapsto \tau$ rescaling and the application of (B 9), the expressions in (B 7) imply

$$\partial_r \sqrt{\frac{A(r, r')}{B(r')}} = \frac{1}{2\lambda B(\dot{r})} \partial_r A(r, \dot{r})$$

$$= \frac{1}{2\lambda B(\dot{r})} \partial_r \left[A(r, \dot{r}) - \lambda^2 B(\dot{r})\right], \tag{B 10}$$

$$\frac{\mathrm{d}}{\mathrm{d}s} \partial_{r'} \sqrt{\frac{A(r, r')}{B(r')}} = \frac{1}{B(\dot{r})} \frac{\mathrm{d}}{\mathrm{d}\tau} \left\{ \frac{B(\dot{r})}{2\lambda} \partial_{r'} \left[A(r, r') - \lambda^2 B(r')\right] \right\}$$

$$= \frac{1}{2\lambda B(\dot{r})} \frac{\mathrm{d}}{\mathrm{d}\tau} \partial_{\dot{r}} \left[A(r, \dot{r}) - \lambda^2 B(\dot{r})\right], \tag{B 11}$$

where, in the first identity, we used the fact that $\partial_r B(\dot{r}) = 0$. Based on these identities, equation (B 3) can be rewritten as

$$\frac{1}{2\lambda B(\dot{r})} \left\{ \partial_r \left[A(r, \dot{r}) - \lambda^2 B(\dot{r})\right] - \frac{\mathrm{d}}{\mathrm{d}\tau} \partial_{\dot{r}} \left[A(r, \dot{r}) - \lambda^2 B(\dot{r})\right] \right\} = 0. \tag{B 12}$$

Since $1/2\lambda B(\dot{r})$ is nonvanishing we obtain from (B 12) that all solutions of (B 3) must satisfy the Euler–Lagrange equation derived from the Lagrangian

$$\mathcal{L}_\lambda(r, \dot{r}) = \frac{1}{2} \left[A(r, \dot{r}) - \lambda^2 B(\dot{r})\right]. \tag{B 13}$$

Therefore, all stationary functions of the functional Q are also stationary functions of the strain energy functional $\mathcal{E}_\lambda$ defined in (2.5) for an appropriate value of λ. This value of λ can be determined from the formula (B 6), which also shows that the corresponding stationary functions of $\mathcal{E}_\lambda$ all satisfy

$$\langle \dot{r}(\tau), C^t_{t_0}(r(\tau))\dot{r}(\tau)\rangle = \lambda^2 \langle \dot{r}(\tau), \dot{r}(\tau)\rangle. \tag{B 14}$$

Therefore, these extrema are null-geodesics of the Lorentzian metric g_λ associated with the generalized Green–Lagrange strain tensor E_λ, as defined in (2.6).

Conversely, assume that $r(\tau)$ is a null-geodesic of g_λ, and hence satisfies both equation (B 12) and (B 14). Reversing the steps leading to (B 14), and employing the inverse rescaling of the independent variable as,

$$\frac{\mathrm{d}s}{\mathrm{d}\tau} = B(\dot{r}(\tau)), \tag{B 15}$$

we obtain the rescaled null-geodesic $r(s)$ is also a solution of the Euler–Lagrange equation (B 3). Therefore, each null-geodesic curve of g_λ is also a stationary function of the functional $Q(\gamma)$, lying on the energy surface $I(r, r') = \lambda$, and hence satisfying the identity (B 6).

Appendix C. Formula for generalized Green–Lagrange null-geodesics

Null-geodesics of the metric g_λ are contained in the zero level set of the first integral $\mathcal{L}_\lambda$. To find the vector field to which such geodesics are tangent, we have to solve the equation

$$\mathcal{L}_\lambda(r, r') = \langle r', E_\lambda(r)r'\rangle = 0. \tag{C 1}$$

We seek the solution of this equation as a unit vector, written as a linear combination of the Cauchy–Green eigenvectors ξ_1 and ξ_2. For later use, we also fix the relative orientation of the eigenvectors as

$$\xi_2(x_0) = \begin{bmatrix} 0 & -1 \\ 1 & 0 \end{bmatrix} \xi_1(x_0). \tag{C 2}$$

Substituting $r' = \alpha\xi_1 + \beta\xi_2$ into (C 1) leads to the equivalent equation

$$\langle \alpha\xi_1 + \beta\xi_2), [C^t_{t_0} - \lambda^2 I](\alpha\xi_1 + \beta\xi_2)\rangle = 0, \tag{C 3}$$

subject to the normalization constraint $\alpha^2 + \beta^2 = 1$.

The expression (C 3) in turn yields the equation

$$\langle (\alpha\xi_1 + \beta\xi_2), (\alpha(\lambda_1 - 1)\xi_1 + \beta(\lambda_2 - 1)\xi_2)\rangle = 0 \tag{C 4}$$

or, equivalently,

$$\alpha^2(\lambda_1 - \lambda^2) + \beta^2(\lambda_2 - \lambda^2) = 0, \tag{C 5}$$

both subject to $\alpha^2 + \beta^2 = 1$, whose solution is

$$\alpha = \pm\sqrt{\frac{\lambda_2 - \lambda^2}{\lambda_2 - \lambda_1}}, \quad \beta = \pm\sqrt{\frac{\lambda^2 - \lambda_1}{\lambda_2 - \lambda_1}}, \tag{C 6}$$

whenever we have

$$\lambda_1 < \lambda^2 < \lambda_2. \tag{C 7}$$

Therefore, the two independent directions forming the light cone at a point x_0 are just $\eta^\pm_\lambda(x_0)$.

We note that for $\lambda = 1$ and for incompressible flows $(\lambda_1 = 1/\lambda_2)$ one obtains

$$\alpha = \pm\sqrt{\frac{1/\lambda_1 - 1}{1/\lambda_1 - \lambda_1}} = \pm\sqrt{\frac{1}{1 + \lambda_1}} \tag{C 8}$$

and

$$\beta = \pm\sqrt{\frac{1 - 1/\lambda_2}{\lambda_2 - 1/\lambda_2}} = \pm\sqrt{\frac{1}{1 + \lambda_2}}, \tag{C 9}$$

thus the vector field in (3.2) takes the specific form

$$\eta_1^{\pm}(x_0) = \frac{1}{\sqrt{1 + \lambda_1(x_0)}}\xi_1(x_0) \pm \frac{1}{\sqrt{1 + \lambda_2(x_0)}}\xi_2(x_0). \tag{C 10}$$

Thus, in incompressible flows, the vector field for primary null-geodesics coincides with the vector field generating lines of maximal Lagrangian shear, obtained in Haller & Beron-Vera (2012) from different considerations.

Appendix D. Existence of Green–Lagrange metric singularities inside coherent Lagrangian vortices

Assume the contrary, i.e., there is no singularity of the metric g_λ inside a photon sphere γ. Since there is no singularity on γ either (by definition), there exists an open neighborhood of γ with no singular points. This in turn implies that there exists a simply connected open set $U_0 \subset \mathbb{R}^2$ that contains γ and its interior, but contains no singularities for the metric g_λ. In that case, (U_0, g_λ) is a simply connected two-dimensional spacetime, homeomorphic to an open disk that contains a closed null-geodesic. But this contradicts a fundamental result in Lorentzian geometry: two-dimensional spacetimes homeomorphic to $\mathbb{R}^2$ (and hence to an open disk in $\mathbb{R}^2$) cannot have closed nonspacelike geodesics (including null-geodesics) (Beem *et al.* 1996).

Appendix E. Finding photon spheres systematically

Assume that $\mathcal{R}_\lambda$ is a limit cycle of the vector field $\eta_\lambda^{\pm}$ for some choice of the sign $\pm$. By the structural stability of limit cycles (Guckenheimer & Holmes 1986), $\mathcal{R}_\lambda$ will smoothly persist under small variations in the parameter λ, giving rise locally to a one-parameter family of limit cycles for the vector field family $\eta_\lambda^{\pm}$. In principle, these limit cycles may deform in an arbitrary fashion, intersect each other, and hence do not necessarily form an annular neighborhood.

Observe, however, that $\eta_\lambda^{\pm}(x_0)$ is a *rotated vector field* in the sense of Duff (1953), which means that each each point x_0, the vector $\eta_\lambda^{\pm}(x_0)$ rotates in the same direction under a change in λ. This property can be verified by noting that the signed projection of the derivative $\frac{\mathrm{d}}{\mathrm{d}\lambda}\eta_\lambda^{\pm}$ on the vector $\eta_\lambda^{\pm}$ has constant sign over the whole domain U_λ.

Indeed, using (C 2), we find that this signed projection of the derivative can be computed as

$$S_\lambda^{\pm}(x_0) = \det\left[\eta_\lambda^{\pm}(x_0), \frac{\mathrm{d}}{\mathrm{d}\lambda}\eta_\lambda^{\pm}(x_0)\right]$$
$$= \frac{\pm\lambda}{\sqrt{(\lambda_2(x_0) - \lambda^2)(\lambda^2 - \lambda_1(x_0))}}, \tag{E 1}$$

and therefore has the same constant sign $\pm$ for all $x_0 \in U_\lambda$ and for any $\lambda > 0$. Note that

sign $S_\lambda^\pm(x_0)$ signals the direction of rotation of $\eta_\lambda^\pm(x_0)$ for increasing λ relative to the positive (counterclockwise) orientation of the $\{\xi_1(x_0), \xi_2(x_0)\}$ basis defined in (C 2).

A remarkable property of limit cycles in rotated families of vector fields is that cycles corresponding to different values of λ do not intersect each other. This statement assumes that the vector field is locally smooth, at least near the limit cycle. In our setting, $\eta_\lambda^\pm$ is generally not smooth globally due to orientational discontinuities. However, $\eta_\lambda^\pm$ can be smoothly oriented in the vicinity of any of its limit cycles, which is enough for the results in Duff (1953) to apply.

We conclude that the limit cycles in the family $\mathcal{R}_\lambda$ grow or shrink under variations of λ, forming annular regions. These annuli of limit cycles may terminate by shrinking to a singularity, shrinking onto a network of separatrices, growing out of the domain U_λ, or by the collision and subsequent disappearance of two cycles through a saddle-node bifurcation (Duff 1953; Perko 2001).

Using (E 1), we obtain

$$\text{sign}\, S_\lambda^\pm(x_0) = \pm\, \text{sign}\, \lambda. \tag{E 2}$$

By the definition of $S_\lambda^\pm(x_0)$, the expression (E 2) determines the sense of rotation of the vector $\eta_\lambda^\pm(x_0)$ at the point x_0 under a small increase in λ. This sense of rotation is measured relative to the positive (counter-clockwise) orientation defined for the Cauchy–Green eigenbasis in (C 2). Specifically, sign $S_\lambda^\pm(x_0) > 0$ refers to counter-clockwise rotation, and sign $S_\lambda^\pm(x_0) < 0$ refers to clockwise rotation.

Following these observations, we can determine the direction in which λ needs to be changed from $\lambda = 1$ in our search for a maximal limit cycle in the vector field family $\eta_\lambda^\pm$. Without loss of generality, we assume that in the eddy candidate region of interest, the trajectories of $\eta_\lambda^\pm$ have a clockwise orientation. If not, reverse their orientation by reversing the directions of the eigenvectors ξ_i defining $\eta_\lambda^\pm$ in (3.2).

Case I: A primary photon sphere exists:
(*a*) Assume that a clockwise oriented, maximal limit cycle $\mathcal{R}_1^+$ of the η_1^+ field is attracting (repelling). Then further limit cycles of the η_λ^+ vector field family can be found outside $\mathcal{R}_1^+$ by increasing (decreasing) the parameter λ from $\lambda = 1$.
(*b*) Assume that a clockwise oriented, maximal limit cycle $\mathcal{R}_1^-$ of the η_1^- field is attracting (repelling). Then further limit cycles of the η_λ^- vector field family can be found outside $\mathcal{R}_1^-$ by decreasing (increasing) the parameter λ from $\lambda = 1$.
Case II: No primary photon sphere exists:
(*a*) Assume that the clockwise oriented η_1^+ field has trajectories forming an inward (outward) spiral. Then limit cycles of the η_λ^+ vector field family may only be found by increasing (decreasing) the parameter λ from $\lambda = 1$.
(*b*) Assume that the clockwise oriented η_1^- field has trajectories forming an inward (outward) spiral. Then limit cycles of the η_λ^- vector field family may only be found by decreasing (increasing) the parameter λ from $\lambda = 1$.

Figure 1 explains the above conclusions for the vector field family η_1^+. The figure shows how changing λ in the appropriate direction results in a rotation of the η_λ^+ vector field, leading to a tighter spiral. This may ultimately lead to the creation of a limit cycle (secondary photon sphere), which is to be tested numerically in each black-hole vortex candidate region. Changing λ in the opposite direction loosens up the spiral and hence cannot create limit cycles.

Theoretically, the maximal photon sphere in a coherent vortex region can be one of two types (Perko 2001). First, it may be a limit cycle of the vector field $\eta_\lambda^\pm$, that reaches the boundary of the domain of definition of $\eta_\lambda^\pm$ for some λ. Alternatively, the maximal photon sphere may actually be a homoclinic or heteroclinic loop of $\eta_\lambda^\pm$, connecting Cauchy-Green
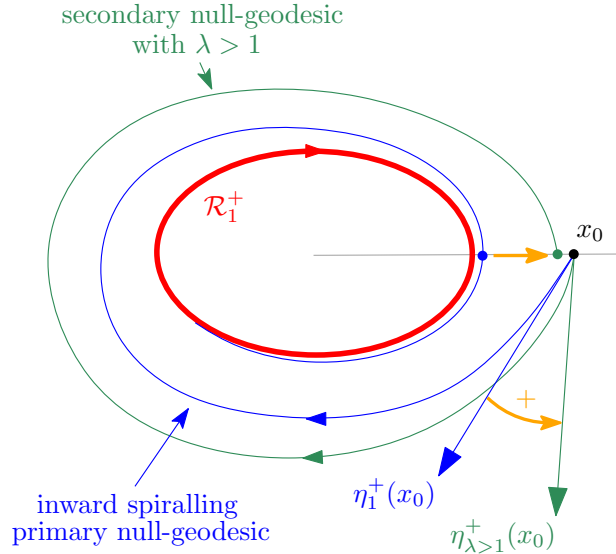
FIGURE 1. Schematics of the search for a secondary photon sphere in a region of spiraling primary null-geodesics. The specific geometry is relevant for the η_λ^+ vector field in the presence of a clockwise inward spiral [Cases I(a) and II(a)]. A primary photon sphere $\mathcal{R}_1^+$ may be present (Case I, shown) or may not be present (Case II). Cases I(b) and II(b) are similar, with the appropriate changes in orientation and in the magnitude of λ relative to one.

singularities to themselves or to each other. In practice, noise in the underlying velocity data and numerical inaccuracies near metric singularities will prevent us from accurately computing such homoclinic or heteroclinic orbits of $\eta_\lambda^\pm$. Instead, we obtain a largest smooth limit cycle when scanning through different values of λ. For a small enough stepsize in varying λ, this largest limit cycle will lie close to the theoretical homoclinic or heteroclinic loop.

Appendix F. Computational steps in the detection of coherent Lagrangian vortices

Our approach to coherent vortex detection can be numerically implemented in the following steps:

(a) Fix a grid $\mathcal{G}_0$ of initial positions and select a time scale T over which ocean rings are to be identified. For each initial condition $x_0 \in \mathcal{G}_0$, integrate the differential equation (2.1) from an initial time t_0 to time $t = t_0 + T$, thereby obtaining a discrete approximation of the flow map $F_{t_0}^t$ over the grid $\mathcal{G}_0$.

(b) Using smaller auxiliary grids around points in $\mathcal{G}_0$, compute the deformation gradient field $\nabla F_{t_0}^t(x_0)$, then the Cauchy–Green strain tensor field $C_{t_0}^t(x_0)$ and its eigenvalue and eigenvector fields, $\lambda_i(x_0)$ and $\xi_i(x_0)$.

(c) Locate singularities of the metric g_1. Such singular points are found where $\lambda_1(x_0) = \lambda_2(x_0) = 1$. For an incompressible flow, metric singularities can be detected as intersections of the level curves $[C_{t_0}^t(x_0)]_{12} = 0$ with the level curves $[C_{t_0}^t(x_0)]_{11} - [C_{t_0}^t(x_0)]_{22} = 0$. Here $[C_{t_0}^t(x_0)]_{ij}$ refers to the (i, j) element of the Cauchy–Green strain tensor.

(d) Locate candidate regions for black-hole eddies whose size is in the range of interest. Specifically, fix a length scale D_0 for eddy diameters of interest, then isolate (clusters of) metric singularities surrounded by singularity-free annular regions of radius larger than D_0.

(*e*) In each black-hole candidate region, construct null geodesics of the Green–Lagrange metric g_1 by solving the differential equations

$$r'(s) = \text{sign}\left\langle \eta_\lambda^\pm(r(s)), \frac{\mathrm{d}r(s-\Delta)}{\mathrm{d}s} \right\rangle \eta_\lambda^\pm(r(s)) \qquad (\text{F 1})$$

for $\lambda = 1$, with Δ denoting the integration step in s. The factor multiplying $\eta_\lambda^\pm(r(s))$ in (F 1) removes orientational discontinuities in $\eta_\lambda^\pm(r(s))$ arising from the lack of a global orientation for $\xi_i(x_0)$; cf. related discussion in Haller & Beron-Vera (2012).

(*f*) In the phase portrait of (F 1) with $\lambda = 1$, use a Poincare section to seek limit cycles of the vector fields $\eta_1^\pm$ (photon spheres of the metric g_1). If such a limit cycle exists, a primary black-hole eddy has been found. The bounding ring of this eddy is obtained by varying λ as discussed in Case I above.

(*g*) If the vector fields $\eta_1^\pm$ admit no limit cycles in the eddy candidate region, then search for the limit cycles of $\eta_\lambda^\pm$ with $\lambda \neq 1$ (secondary photon spheres). This is done by following the procedure described in Case II above. If a limit cycle is found, a secondary black-hole eddy has been located. Then seek the largest possible limit cycles in the candidate region as the ring bounding the eddy. The eddy is strengthening if its limit cycles exist for $\lambda < 1$, and weakening, if the cycles exist for $\lambda > 1$. If no limit cycle is found, the candidate region is not a black-hole eddy.

(*h*) To track the motion of black-hole eddies in time, find their time t positions by applying the flow map $F_{t_0}^t$ to their bounding rings identified at time t_0.

Appendix G. Data set and numerical methods for the Agulhas leakage

In locating black-hole eddies from observational ocean data, fluid particles are assumed to obey a differential equation of the form (2.1) with the velocity field given by

$$v(x,t) = \left(-\frac{g}{f(x^2)} \frac{\partial h(x,t)}{\partial x^2}, \frac{g}{f(x^2)} \frac{\partial h(x,t)}{\partial x^1} \right). \qquad (\text{G 1})$$

Here $x = (x^1, x^2)$ denotes a position on a β-plane with Cartesian zonal x^1 and meridional x^2 coordinate; the function $h(x,t)$ denotes the SSH field as a function of location and time; $f(x^2)$ is the Coriolis parameter (twice the local vertical component of the Earth's angular velocity); and g denotes the constant of gravity.

The background component of the field $h(x,t)$ is steady. It is obtained from a mean dynamic topography constructed from altimetry data, in-situ measurements, and a geoid model. The perturbation component of the $h(x,t)$ field is transient, given by altimetric SSH anomaly measurements provided weekly on a 0.25°-resolution longitude–latitude grid. The perturbation component is relative to a 7-year (1993–1999) mean, obtained from the combined processing of a constellation of available altimeters. For more detail on the data, we refer the reader to Beron-Vera *et al.* (2013).

We select a regular grid $\mathcal{G}_0$ of 1000^2 initial conditions, with the initial time chosen as $t_0 = 24$ November 2006, and with the final time chosen as $t = t_0 + 3$ months. We employ a smaller auxiliary grid around each point in $\mathcal{G}_0$ for the purposes of finite-differencing the flow map $F_{t_0}^t$. Trajectory integration is performed by a variable stepsize fourth-order Runge–Kutta method, with cubic interpolations of the altimetry velocity field between grid points.

Admissible regions for black-hole eddies are located as described in steps (*c*)–(*d*) of the relativistic eddy detection algorithm outlined above. We show the eight candidate
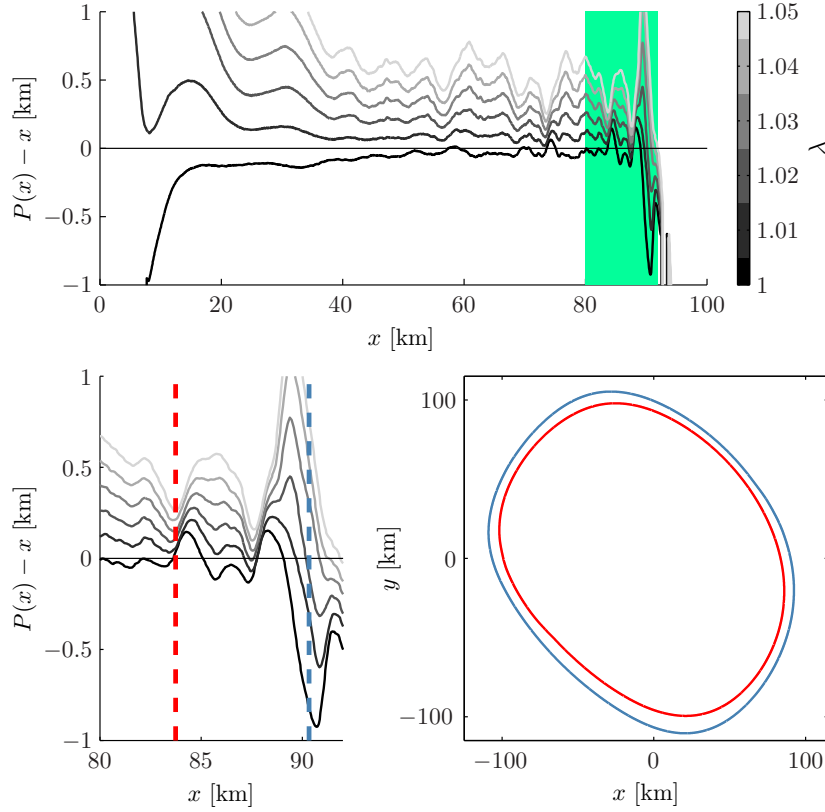
FIGURE 2. Identification of a primary black-hole eddy in region 2 of Figure 3. (top panel) The Poincare map for various values of the parameter λ, computed for the η_λ^+ vector field family. Note that $\lambda = 1$ already yields a fixed point for the map, and hence a primary black-hole eddy exists. The parameter λ is then increased from $\lambda = 1$, following the procedure described in step (f) of the relativistic eddy detection algorithm. (bottom-left panel) Blow-up of the green region of the upper panel, ranging from 80 to 92 km along the Poincare section. Red dashed line marks the location of the maximal fixed point for $\lambda = 1$. Blue dashed line marks the maximal fixed point of the whole map family, obtained for $\lambda = 1.02$. (Fixed points in the highest 5km range are discounted because of their numerical sensitivity.) (bottom-right panel) the corresponding primary photon sphere (red) and ring (blue).

regions obtained in this fashion for our data set in Figure 3. With the candidate regions (a)–(h) located, we use a finer grid of initial conditions along a one-dimensional Poincare section in each region to integrate trajectories of (F 1), and hence compute the first return map (Poincare map) to the section. We tested several grid resolutions on the most noisy candidate regions before fixing a resolution of 2500 grid points. At this resolution, the Poincare maps showed overall convergence in all regions. In some cases, thin strips of roughly 5 km near the exterior boundary of the domain of definition of the Poincare map still showed a lack of convergence. These domains contain initial conditions passing very close to metric singularities, which results in high numerical sensitivities in trajectory integration. We have excluded these small domains from our computations, and selected the maximal photon spheres outside them as eddy boundaries.

The process of identifying the ring boundary from the outermost fixed point of the Poincare map in region 2 is shown in Figure 2. This black-hole eddy was obtained from the analysis of the η_λ^+ vector field. The η_λ^- vector field admits no limit cycles in region 2.

The procedure summarized in Figure 3 for region 2 was carried out for all the eight black-hole region candidates shown in the upper panel of Figure 3. The results of the analysis are shown in the middle panel of the same figure.

REFERENCES

BEEM, J. K., EHRLICH, P. L. & KEVIN, L. E. 1996 *Global Lorentzian Geometry*. Boca Raton: CRC Press.

BERON-VERA, F. J., WANG, Y., OLASCOAGA, M. J., GONI, G. J. & HALLER, G. 2013 Objective detection of oceanic eddies and the Agulhas leakage. *J. Phys. Oceanogr.* **43**, 1426–1438.

DUFF, G. F. D. 1953 Limit cycles and rotated vector fields. *Ann. Math.* **57**, 15–31.

GELFAND, I. A. & FOMIN, S. V. 2000 *Calculus of Variations*. Dover Publications.

GUCKENHEIMER, J. & HOLMES, P. 1986 *Nonlinear Oscillations, Dynamical Systems, and Bifurcations of Vector Fields*. New York: Springer.

HALLER, G. & BERON-VERA, F. J. 2012 Geodesic theory of transport barriers in two-dimensional flows. *Physica D* **241**, 1680–1702.

PERKO, L. 2001 *Differential Equations and Dynamical Systems*. New York: Springer.